Orbital Angular Momentum Multiplexed Deterministic All-Optical Quantum Erasure-Correcting Code

Yanbo Lou,[1] Yinghui Lv,[1] Jiabin Wang,[1] Shengshuai Liu,[1,*] and Jietai Jing[1,2,3,†]
[1]State Key Laboratory of Precision Spectroscopy, Joint Institute of Advanced Science and Technology, School of Physics and Electronic Science, East China Normal University, Shanghai 200062, China
[2]CAS Center for Excellence in Ultra-intense Laser Science, Shanghai 201800, China
[3]Collaborative Innovation Center of Extreme Optics, Shanxi University, Taiyuan, Shanxi 030006, China

(Received 7 January 2023; revised 30 September 2023; accepted 19 December 2023; published 23 January 2024)

Quantum erasure-correcting code, which corrects the erasure in the transmission of quantum information, is an important protocol in quantum information. In the continuous variable regime, the feed-forward technique is needed for realizing quantum erasure-correcting code. This feed-forward technique involves optic-electro and electro-optic conversions, limiting the bandwidth of quantum erasure-correcting code. Moreover, in the previous continuous variable quantum erasure-correcting code, only two modes are protected against erasure, limiting the applications of quantum erasure-correcting code in high-capacity quantum information processing. In this Letter, by utilizing the orbital angular momentum (OAM) multiplexed entanglement in the encoding part and replacing the feed-forward technique with OAM mode-matched phase-sensitive amplifier in the decoding part, we experimentally demonstrate a scheme of OAM multiplexed deterministic all-optical quantum erasure-correcting code. We experimentally demonstrate that four orthogonal modes can be simultaneously protected against one arbitrary erasure. Our results provide an all-optical platform to implement quantum erasure-correcting code and may have potential applications in implementing all-optical fault-tolerant quantum information processing.

DOI: 10.1103/PhysRevLett.132.040601

Quantum information protocols [1,2], which transfer and manipulate information by utilizing quantum resources, have the ability to significantly improve the fidelity, capacity, and security of information processing. Therefore, quantum information protocols have been widely studied and constructed both in the discrete variable and continuous variable (CV) regimes, including quantum key distribution [3,4], quantum teleportation [5–8], quantum cloning [9–13], and so on. In quantum information protocols, errors will inevitably be introduced in the process of manipulating quantum information because quantum information is fragile [14]. In this sense, quantum error correction [15–20], which can efficiently correct errors in quantum information protocols, is indispensable.

In quantum information protocols, one type of error is erasure. This error is induced by the erasure of quantum information in the transmission channel. To correct this erasure, quantum erasure-correcting code (QECC) was first considered and studied in the discrete variable regime [21–23] and then transplanted to the CV regime [24–27]. In the CV regime, QECC is studied both in theory [24,26,27] and experiment [25]. As mentioned in Ref. [25], when one transmission channel erases information completely, QECC can protect transferred quantum states against such erasure, ensuring reliable quantum state transfer. However, in the CV regime, QECC [24,25] is based on the feed-forward technique, which involves the optic-electro and electro-optic conversions. These conversions limit the bandwidth of QECC. Therefore, the all-optical QECC (AOQECC), which replaces feed-forward technique with optical amplifier [24], needs to be explored for broadening the bandwidth of QECC. Moreover, in the experiment of Ref. [25], only one vacuum mode and one coherent mode are protected in the transmission channel, which limits its applications in high-capacity quantum information processing. In this Letter, we experimentally demonstrate orbital angular momentum (OAM) multiplexed [28–33] deterministic AOQECC, which simultaneously protects four orthogonal modes in two input states from one arbitrary erasure. For our AOQECC, the originality is utilizing the OAM multiplexed CV entanglement in the encoding part and replacing the feed-forward technology with OAM mode-matched phase-sensitive amplifier (PSA) based on four-wave mixing (FWM) process [34–38] in the decoding part.

Figure 1 shows the schematics of the experimental setup for implementing OAM multiplexed deterministic AOQECC. OAM multiplexed Einstein-Podolsky-Rosen (EPR) entangled source [39] is generated based on double-Λ configuration FWM process [34–38]. As shown in Fig. 1(b), in this FWM process, two pump photons convert to one photon for EPR1, which is red detuned from the pump beam, and one photon for EPR2, which is blue detuned from the pump beam. The Hamiltonian of such FWM process can be given by [31]

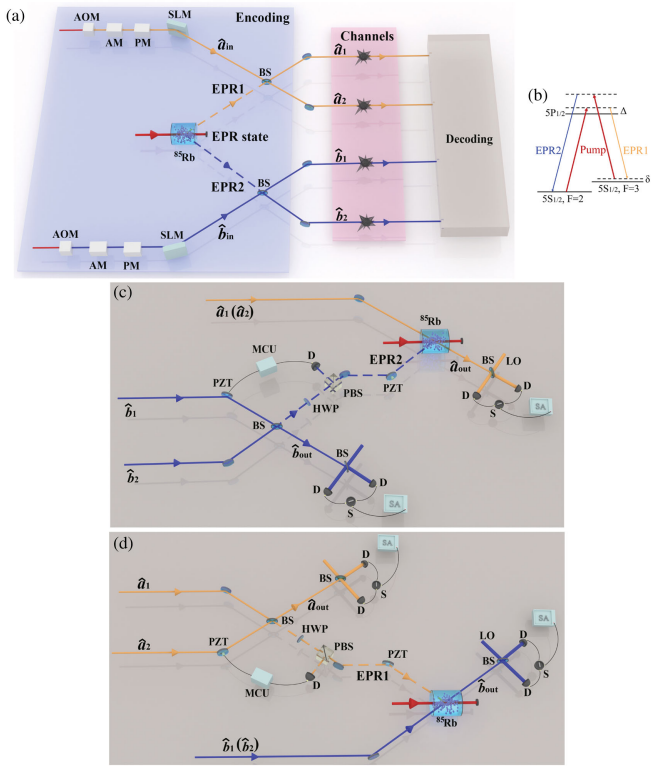

FIG. 1. The experimental setup of OAM multiplexed deterministic AOQECC. (a) The experimental scheme. One OAM-superposition-mode coded input state $\hat{a}_{\rm in}$ ($\hat{b}_{\rm in}$), which is red-shifted (blue-shifted) 3.04 GHz from the pump beam, is obtained by passing one beam from the laser through acousto-optic modulator (AOM), amplitude modulator (AM), phase modulator (PM), and spatial light modulator (SLM). (b) Energy level diagram of the double-Λ configuration. Δ, one-photon detuning; δ, two-photon detuning. (c) The decoding device when $\hat{a}_1$ or $\hat{a}_2$ is erased. A piezoelectric transducer (PZT) is placed in the path of $\hat{b}_1$ for locking the relative phase between $\hat{b}_1$ and $\hat{b}_2$. We pass one of the output beams from 50:50 beam splitter (BS) through a 99:1 BS consisted by a half-wave plate (HWP) and a polarization beam splitter (PBS). Such 1% of the beam is detected by a photodetector (D). Then, the direct current component of D is sent to a microcontrol unit (MCU) [40] to lock the relative phase between $\hat{b}_1$ and $\hat{b}_2$. (d) The decoding device when $\hat{b}_1$ or $\hat{b}_2$ is erased. ^{85}Rb, ^{85}Rb vapor cell; EPR state, OAM multiplexed Einstein-Podolsky-Rosen (EPR) entangled source; $\hat{a}_{\rm in}$ and $\hat{b}_{\rm in}$, the annihilation operators associated with the input coherent states; $\hat{a}_1$, $\hat{a}_2$, $\hat{b}_1$, and $\hat{b}_2$, the annihilation operators associated with four-mode code, respectively; SA, spectrum analyzer; LO, local oscillator; $\hat{a}_{\rm out}$ and $\hat{b}_{\rm out}$, the annihilation operators associated with the output states. The experimental details of experimental setup are shown in Sec. A of the Supplemental Material [41].

$$\hat{H} = i\hbar\sum_{\ell}\gamma_{\ell}\hat{a}^{\dagger}_{{\rm EPR1},\ell}\hat{a}^{\dagger}_{{\rm EPR2},-\ell} + {\rm H.c.}, \tag{1}$$

where $\hat{a}^{\dagger}_{{\rm EPR1},\ell}$ ($\hat{a}^{\dagger}_{{\rm EPR2},-\ell}$) is the creation operator associated with OAM mode in EPR1 (EPR2). ℓ ($-\ell$) is topological charge. γ_{ℓ} denotes the interaction strength of each pair of Laguerre-Gauss (LG) modes in FWM process. Because ${\rm LG}_{\ell}$ and ${\rm LG}_{-\ell}$ have the same beam size, $\gamma_{\ell} = \gamma_{-\ell}$. Therefore, the corresponding intensity gain of the FWM process $H = \cosh^2(\gamma_{\ell}\tau) = \cosh^2(\gamma_{-\ell}\tau)$, where τ is the interaction timescale. To encode the input states, two input states ($\hat{a}_{\rm in} = (1/\sqrt{2})\hat{a}_{{\rm in},\ell} + (1/\sqrt{2})\hat{a}_{{\rm in},-\ell}$ and $\hat{b}_{\rm in} = (1/\sqrt{2})\hat{b}_{{\rm in},\ell} + (1/\sqrt{2})\hat{b}_{{\rm in},-\ell}$) are mixed with OAM multiplexed EPR entangled pair by two 50:50 beam splitters (BSs). In this way, four-mode code, which contains four beams $\hat{a}_1$, $\hat{a}_2$, $\hat{b}_1$, and $\hat{b}_2$, is formed. Because the different OAM modes are orthogonal with each other, only OAM matched multiplexed EPR entangled pair can be introduced to four-mode code by 50:50 BS and the topological charges of $\hat{a}_1$ and $\hat{a}_2$ ($\hat{b}_1$ and $\hat{b}_2$) are the same as $\hat{a}_{\rm in}$ ($\hat{b}_{\rm in}$). Then, these four beams are sent to transmission channels, respectively.

In OAM multiplexed deterministic AOQECC protocol, the information of one of the transmission channels can be completely blocked, i.e., erasure. If mode $\hat{a}_1$ is lost during the transmission through the channel, as shown in Fig. 1(c), the decoder combines $\hat{b}_1$ and $\hat{b}_2$ with a 50:50 BS. After locking the relative phase between $\hat{b}_1$ and $\hat{b}_2$, the 50:50 BS has one bright output and one dark output. The bright output $\hat{b}_{\rm out}$ is exactly the input state $\hat{b}_{\rm in}$, while the dark output is EPR2. In other words, $\hat{b}_{\rm in}$ can be recovered almost perfectly in this case. Then, the decoder amplifies $\hat{a}_2$ through an OAM mode-matched PSA with the help of EPR2 when the intensity gain of PSA G is set to 2. Because of the OAM conservation of this FWM process [32], the EPR state, whose topological charge is opposite to $\hat{a}_2$, can be introduced to output state $\hat{a}_{\rm out}$ through this OAM mode-matched amplification [31]. After such amplification, $\hat{a}_{\rm out}$ (i.e., the amplified $\hat{a}_2$) can be expressed as

$$\begin{aligned}\hat{a}_{\rm out} &= \sqrt{G}\hat{a}_2 + \sqrt{G-1}\hat{a}^{\dagger}_{\rm EPR2}e^{-i\theta},\\ &= \frac{1}{\sqrt{2}}(\hat{a}_{{\rm in},\ell} + \hat{a}_{{\rm in},-\ell}) + \frac{1}{\sqrt{2}}(\hat{a}^{\dagger}_{{\rm EPR2},-\ell}e^{-i\theta} - \hat{a}_{{\rm EPR1},\ell})\\ &\quad + \frac{1}{\sqrt{2}}(\hat{a}^{\dagger}_{{\rm EPR2},\ell}e^{-i\theta} - \hat{a}_{{\rm EPR1},-\ell}),\end{aligned} \tag{2}$$

where θ is the relative phase between EPR1 and EPR2. When the relative phase between EPR1 and EPR2 is 0 and the intensity gain of the FWM for generating EPR entanglement is much greater than 1, the last two terms in Eq. (2) will be reduced to 0. In this way, the decoder can recover $\hat{a}_{\rm in}$ almost perfectly. The details of theoretical calculation are shown in Sec. B of the Supplemental Material [41].

To quantify the recovered state of OAM multiplexed deterministic AOQECC protocol, the fidelity, which is defined as the overlap between the density matrix of input and output states, is utilized. For a coherent state, the fidelity is given by [45]

$$F = \frac{2}{\sigma_Q}\exp\left[-\frac{2}{\sigma_Q}|\beta_{\text{out}} - \beta_{\text{in}}|^2\right], \tag{3}$$

where σ_Q is the variance of the recovered state in representation of the Q function and $\sigma_Q = \sqrt{(1+\sigma_W^{\hat{X}})(1+\sigma_W^{\hat{Y}})}$. $\hat{X}$ ($\hat{X} = \hat{a}^\dagger + \hat{a}$) and $\hat{Y}$ ($\hat{Y} = i\hat{a}^\dagger - i\hat{a}$) are the amplitude quadrature and phase quadrature of the recovered state, respectively. $\sigma_W^{\hat{X}}$ ($\sigma_W^{\hat{Y}}$) is the corresponding fluctuation variance. β_{in} (β_{out}) is the amplitude of the input (output) state at encoding (decoding) station. Because of $\hat{b}_{\text{out}} = \hat{b}_{\text{in}}$, the fidelity of the output state $\hat{b}_{\text{out}}$ is 1. Based on Eqs. (1) to (3), we can calculate the fidelity of the output state $\hat{a}_{\text{out}}$ as

$$\begin{aligned} F &= \frac{2}{\sqrt{(2+A+B)(2+C+D)}}, \\ &= \frac{1}{2H - 2\sqrt{H(H-1)}}. \end{aligned} \tag{4}$$

$A = \frac{1}{2}\Delta^2(\hat{X}_{\hat{a}_{\text{EPR2},-\ell}} - \hat{X}_{\hat{a}_{\text{EPR1},\ell}})$, $B = \frac{1}{2}\Delta^2(\hat{X}_{\hat{a}_{\text{EPR2},\ell}} - \hat{X}_{\hat{a}_{\text{EPR1},-\ell}})$, $C = \frac{1}{2}\Delta^2(\hat{Y}_{\hat{a}_{\text{EPR2},-\ell}} + \hat{Y}_{\hat{a}_{\text{EPR1},\ell}})$, and $D = \frac{1}{2}\Delta^2(\hat{Y}_{\hat{a}_{\text{EPR2},\ell}} + \hat{Y}_{\hat{a}_{\text{EPR1},-\ell}})$. Based on Eq. (4), it can be seen that the fidelity of the reconstructed output state $\hat{a}_{\text{out}}$ highly depends on the initial EPR entanglement degree generated by the FWM process and only the entanglement with mode matched to the OAM modes of inputs can affect fidelity. Moreover, when $H \gg 1$ (the degree of EPR squeezing approaches infinite), $F \approx 1$. In other words, although one transmission channel is completely blocked (the maximum possible quantum correlation will be severely reduced), the fidelity of the recovered two outputs in our scheme can approach 1 in principle if the initial EPR entanglement degree is high enough. By the same token, we can obtain the corresponding models for losing other modes or changing inputs to $\hat{a}_{\text{in}} = (1/\sqrt{2})\hat{a}_{\text{in},\ell} - (1/\sqrt{2})\hat{a}_{\text{in},-\ell}$ and $\hat{b}_{\text{in}} = (1/\sqrt{2})\hat{b}_{\text{in},\ell} - (1/\sqrt{2})\hat{b}_{\text{in},-\ell}$.

To examine the amplitudes of all the input and output, we modulate signals on the amplitude quadrature ($\hat{X}$) and the phase quadrature ($\hat{Y}$) of the two input states at 1.5 MHz radio frequency by using amplitude modulator (AM) and phase modulator (PM) as shown in Fig. 1(a) [13]. To measure the fidelity of OAM multiplexed deterministic AOQECC protocol, two balanced homodyne detections (BHDs) are utilized. The detector of BHD has a transimpedance gain of 10^5 V/A and quantum efficiency of about 97%. The spectrum analyzer (SA) is used to analyze the amplitude quadrature variance (locking the phase of BHD to 0) and phase quadrature variance (locking the phase of BHD to $\pi/2$) of the recovered states ($\hat{a}_{\text{out}}$ and $\hat{b}_{\text{out}}$). The phase locking is realized by a microcontrol unit (MCU).

The typical noise power results at 1.5 MHz with erasure on $\hat{a}_1$ channel, while the input states carrying OAM superposition mode ($\hat{a}_{\text{in}} = (1/\sqrt{2})\hat{a}_{\text{in},1} + (1/\sqrt{2})\hat{a}_{\text{in},-1}$ and $\hat{b}_{\text{in}} = (1/\sqrt{2})\hat{b}_{\text{in},1} + (1/\sqrt{2})\hat{b}_{\text{in},-1}$ or $\hat{a}_{\text{in}} = (1/\sqrt{2})\hat{a}_{\text{in},1} - (1/\sqrt{2})\hat{a}_{\text{in},-1}$ and $\hat{b}_{\text{in}} = (1/\sqrt{2})\hat{b}_{\text{in},1} - (1/\sqrt{2})\hat{b}_{\text{in},-1}$), are shown in Fig. 2. The corresponding experimental results for examining the amplitudes of the input and output are shown in Sec. C of the Supplemental Material [41]. The amplitudes of input and output are almost equal for all these cases. When $\hat{a}_{\text{in}} = (1/\sqrt{2})\hat{a}_{\text{in},1} + (1/\sqrt{2})\hat{a}_{\text{in},-1}$, as shown in Figs. 2(a) and 2(b), green traces are the measured amplitude quadrature variance and phase quadrature variance of $\hat{a}_{\text{in}}$. To obtain the classical limit, we block the OAM multiplexed EPR entanglement. The measured amplitude quadrature variance and phase quadrature variance [blue traces in Fig. 2(a) and

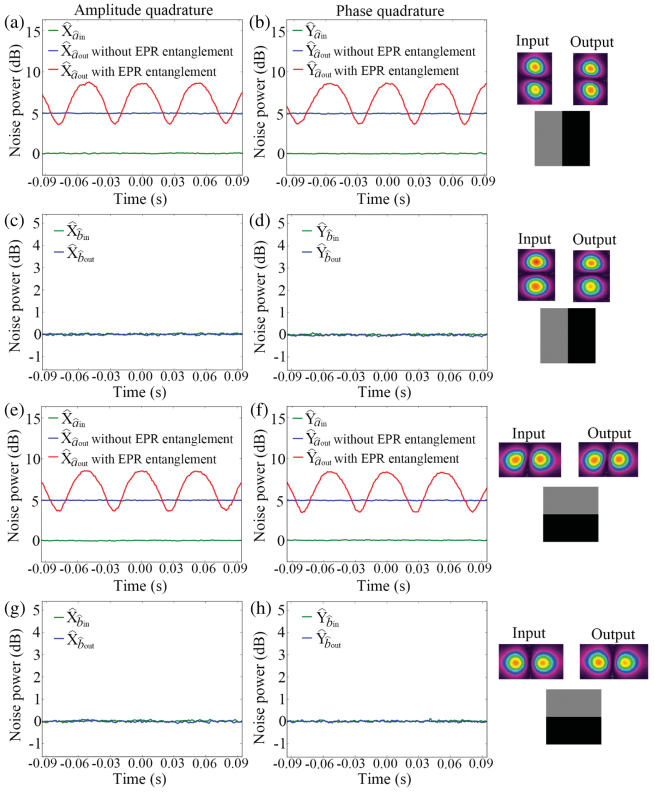

FIG. 2. The typical noise power results for correcting the erasure on $\hat{a}_1$ channel. (a) The amplitude quadrature variances for the input state $\hat{a}_{\text{in}}$ (green trace) and the output state $\hat{a}_{\text{out}}$ (red trace) at 1.5 MHz when $\hat{a}_{\text{in}} = (1/\sqrt{2})\hat{a}_{\text{in},1} + (1/\sqrt{2})\hat{a}_{\text{in},-1}$, respectively. The corresponding classical limit is shown as blue trace. (b) The phase quadrature variances for the input state $\hat{a}_{\text{in}}$ and the output state $\hat{a}_{\text{out}}$ at 1.5 MHz. (c) The amplitude quadrature variances for the input state $\hat{b}_{\text{in}}$ (green trace) and the output state $\hat{b}_{\text{out}}$ (blue trace) at 1.5 MHz when $\hat{b}_{\text{in}} = (1/\sqrt{2})\hat{b}_{\text{in},1} + (1/\sqrt{2})\hat{b}_{\text{in},-1}$, respectively. (d) The phase quadrature variances for the input state $\hat{b}_{\text{in}}$ and the output state $\hat{b}_{\text{out}}$ at 1.5 MHz. (e) and (f) are the corresponding results for $\hat{a}_{\text{in}}$ and $\hat{a}_{\text{out}}$ when $\hat{a}_{\text{in}} = (1/\sqrt{2})\hat{a}_{\text{in},1} - (1/\sqrt{2})\hat{a}_{\text{in},-1}$. (g) and (h) are the corresponding results for $\hat{b}_{\text{in}}$ and $\hat{b}_{\text{out}}$ when $\hat{b}_{\text{in}} = (1/\sqrt{2})\hat{b}_{\text{in},1} - (1/\sqrt{2})\hat{b}_{\text{in},-1}$. The right insets are the computer-generated holograms for $\text{LG}_1 + \text{LG}_{-1}$ and $\text{LG}_1 - \text{LG}_{-1}$ and the corresponding images of input and output fields, respectively.

Fig. 2(b)] are 4.89 ± 0.11 dB and 4.89 ± 0.12 dB above the corresponding quadrature variances of the input state, respectively. This gives a fidelity of classical limit 0.49 ± 0.01. The red trace in Fig. 2(a) [Fig. 2(b)] is the measured amplitude (phase) quadrature variance of the recovered state $\hat{a}_{\mathrm{out}}$ by scanning the relative phase θ between EPR1 and EPR2. When θ is 0, the red trace reaches the minimum. In this sense, the minima of each red trace can be treated as the variance of $\hat{X}_{\hat{a}_{\mathrm{out}}}$ ($\hat{Y}_{\hat{a}_{\mathrm{out}}}$) of the output state. As shown in Figs. 2(a) and 2(b), the variances of $\hat{X}_{\hat{a}_{\mathrm{out}}}$ and $\hat{Y}_{\hat{a}_{\mathrm{out}}}$ quadratures are 3.56 ± 0.13 dB and 3.60 ± 0.14 dB above the corresponding quadrature variances of the input state, respectively. In this sense, we can calculate the fidelity of the recovered state, which is 0.61 ± 0.01, beating the corresponding classical limit of 0.49 ± 0.01. The green trace and blue trace in Fig. 2(c) [Fig. 2(d)] are the measured amplitude (phase) quadrature variances of the input $\hat{b}_{\mathrm{in}}$ measured by another BHD and output $\hat{b}_{\mathrm{out}}$ when $\hat{b}_{\mathrm{in}} = (1/\sqrt{2})\hat{b}_{\mathrm{in},1} + (1/\sqrt{2})\hat{b}_{\mathrm{in},-1}$, respectively. This gives the fidelity of about 1. Based on Figs. 2(e) and 2(f), we can calculate that the fidelity of the recovered state $\hat{a}_{\mathrm{out}}$ when $\hat{a}_{\mathrm{in}} = (1/\sqrt{2})\hat{a}_{\mathrm{in},1} - (1/\sqrt{2})\hat{a}_{\mathrm{in},-1}$, which is 0.62 ± 0.01, beating the corresponding classical limit of 0.49 ± 0.01. Based on Figs. 2(g) and 2(h), we can calculate the fidelity of recovered state $\hat{b}_{\mathrm{out}}$ when $\hat{b}_{\mathrm{in}} = (1/\sqrt{2})\hat{b}_{\mathrm{in},1} - (1/\sqrt{2})\hat{b}_{\mathrm{in},-1}$, which is about 1. In addition, the computer-generated hologram for $\mathrm{LG}_1 + \mathrm{LG}_{-1}$ ($\mathrm{LG}_1 - \mathrm{LG}_{-1}$) and the corresponding images of input and output fields are shown on the right side of Fig. 2. These images clearly show that the spatial optical modes carried by the recovered states are almost the same as the two inputs. Based on the OAM multiplexed entanglement results in Sec. D of Supplemental Material [41] and Eq. (4), we can obtain the corresponding theoretical fidelity of reconstructed output state $\hat{a}_{\mathrm{out}}$, which is 0.64 ± 0.01. This is close to our experimental results. The slight difference is mainly caused by the extra noise introduced by OAM mode-matched PSA. Moreover, we also measure the noise power results for correcting the erasure on $\hat{a}_1$ channel when $\hat{a}_{\mathrm{in}} = \hat{a}_{\mathrm{in},1}$ and $\hat{b}_{\mathrm{in}} = \hat{b}_{\mathrm{in},-1}$ ($\hat{a}_{\mathrm{in}} = \hat{a}_{\mathrm{in},-1}$ and $\hat{b}_{\mathrm{in}} = \hat{b}_{\mathrm{in},1}$), and demonstrate that our scheme is also applicable to OAM modes (Sec. E of the Supplemental Material [41]).

The results with erasure on $\hat{a}_2$, $\hat{b}_1$, and $\hat{b}_2$ channels are similar to Fig. 2, which are shown in Secs. F–H of the Supplemental Material [41]. All these results clearly show that OAM multiplexed deterministic AOQECC can protect four orthogonal modes in two inputs ($\hat{a}_{\mathrm{in}}$ and $\hat{b}_{\mathrm{in}}$) from one erasure in any of the four channels.

To show the bandwidth of our OAM multiplexed deterministic AOQECC protocol, which is induced by avoiding feed-forward technique, we scan the analysis frequency from 1.2 to 2.7 MHz and measure the fidelities for two recovered states as shown in Fig. 3. We select such a sideband frequency range due to the extra classical noise

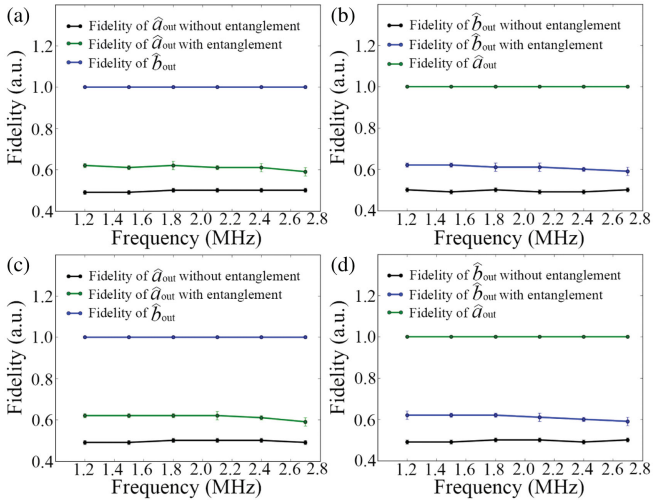

FIG. 3. The relationship between fidelities and the sideband frequency. (a) [(c)] When $\hat{a}_{\mathrm{in}} = (1/\sqrt{2})\hat{a}_{\mathrm{in},1} + (1/\sqrt{2})\hat{a}_{\mathrm{in},-1}$ [$\hat{a}_{\mathrm{in}} = (1/\sqrt{2})\hat{a}_{\mathrm{in},1} - (1/\sqrt{2})\hat{a}_{\mathrm{in},-1}$], the fidelities of $\hat{a}_{\mathrm{out}}$, the corresponding classical limit, and $\hat{b}_{\mathrm{out}}$ with erasure on $\hat{a}_1$ channel are shown as the green, black, and blue traces, respectively. (b) [(d)] When $\hat{b}_{\mathrm{in}} = (1/\sqrt{2})\hat{b}_{\mathrm{in},1} + (1/\sqrt{2})\hat{b}_{\mathrm{in},-1}$ [$\hat{b}_{\mathrm{in}} = (1/\sqrt{2})\hat{b}_{\mathrm{in},1} - (1/\sqrt{2})\hat{b}_{\mathrm{in},-1}$], the fidelities of $\hat{b}_{\mathrm{out}}$, the corresponding classical limit, and $\hat{a}_{\mathrm{out}}$ with erasure on $\hat{b}_1$ channel are shown as the blue, black, and green traces, respectively. The error bars are obtained from the standard deviations of multiple repeated measurements.

from the laser in low sideband frequency and the rf output frequency response limitation of the photodetector. The fidelities of $\hat{a}_{\mathrm{out}}$ and $\hat{b}_{\mathrm{out}}$ with erasure on $\hat{a}_1$ ($\hat{b}_1$) channel are shown as green traces and blue traces in Figs. 3(a) and 3(c) [Figs. 3(b) and 3(d)], respectively. The corresponding classical limits are shown as the black traces in Fig. 3. From 1.2 to 2.7 MHz, we can see that the fidelities of recovered state $\hat{a}_{\mathrm{out}}$ and $\hat{b}_{\mathrm{out}}$ can beat the corresponding classical limit, which clearly shows that OAM multiplexed deterministic AOQECC protocol can be successfully implemented within this bandwidth. The slight decrease of the fidelity as the increase of analysis frequency is due to the decrease of the squeezing of the EPR entangled source. These results are proof-of-principle demonstration of AOQECC, and show the advantage of the all-optical architecture. In addition, the bandwidth of our AOQECC protocol is mainly determined by the bandwidth of EPR entanglement. To improve the bandwidth of AOQECC, one could use other broadband EPR entanglement to perform AOQECC protocol. Recently, the THz sideband CV squeezing based on the periodically poled LiNbO3 waveguide has been successfully demonstrated [46], with which the ultrabroadband AOQECC is promising to be demonstrated in the future.

Because the fidelity of AOQECC is mainly determined by the squeezing of the EPR entangled source, to increase the fidelity of our protocol in the future, we need to find

possible ways to improve the squeezing. First, we could modulate the internal energy level with additional lasers [47]. Second, we could further decrease the losses of our system, including decreasing the losses of optical components, increasing the quantum efficiency of photodetectors, and optimizing the balance of BS in BHD [48]. Third, entanglement purification could also be utilized in our system. For the recent experiments, the state-of-the-art value of squeezing is 15 dB [49], the state-of-the-art value of EPR squeezing is about 11 dB [48]. With such a EPR squeezing level, a fidelity of about 0.93 can be achieved.

To conclude, we have experimentally implemented OAM multiplexed deterministic AOQECC protocol. We demonstrate that four orthogonal modes in two inputs ($\hat{a}_{\mathrm{in}}$ and $\hat{b}_{\mathrm{in}}$) can be simultaneously protected from one erasure in any of the four channels. The fidelities of all situations can beat the corresponding classical limits. Moreover, we have shown that in the bandwidth of 1.2 to 2.7 MHz, OAM multiplexed deterministic AOQECC can be successfully implemented. Our results provide a promising platform to implement all-optical fault-tolerant quantum information processing.

This work was funded by the National Natural Science Foundation of China (12225404, 11874155, 91436211, 11374104, 12174110); Innovation Program of Shanghai Municipal Education Commission (Grant No. 2021-01-07-00-08-E00100); Program of Shanghai Academic Research Leader (22XD1400700); Basic Research Project of Shanghai Science and Technology Commission (20JC1416100); Natural Science Foundation of Shanghai (17ZR1442900); Minhang Leading Talents (201971); Shanghai Sailing Program (21YF1410800); Natural Science Foundation of Chongqing (CSTB2022NSCQ-MSX0893); Shanghai Municipal Science and Technology Major Project (2019SHZDZX01); the 111 project (B12024).

*Corresponding author: ssliu@lps.ecnu.edu.cn
†Corresponding author: jtjing@phy.ecnu.edu.cn

[1] S. L. Braunstein and P. van Loock, Rev. Mod. Phys. **77**, 513 (2005).
[2] A. Galindo and M. A. Martín-Delgado, Rev. Mod. Phys. **74**, 347 (2002).
[3] V. Scarani, H. Bechmann-Pasquinucci, N. J. Cerf, M. Dušek, N. Lütkenhaus, and M. Peev, Rev. Mod. Phys. **81**, 1301 (2009).
[4] F. Xu, X. Ma, Q. Zhang, H.-K. Lo, and J.-W. Pan, Rev. Mod. Phys. **92**, 025002 (2020).
[5] C. H. Bennett, G. Brassard, C. Crépeau, R. Jozsa, A. Peres, and W. K. Wootters, Phys. Rev. Lett. **70**, 1895 (1993).
[6] D. Bouwmeester, J.-W. Pan, K. Mattle, M. Eibl, H. Weinfurter, and A. Zeilinger, Nature (London) **390**, 575 (1997).
[7] S. L. Braunstein and H. J. Kimble, Phys. Rev. Lett. **80**, 869 (1998).
[8] A. Furusawa, J. L. Sorensen, S. L. Braunstein, C. A. Fuchs, H. J. Kimble, and E. S. Polzik, Science **282**, 706 (1998).
[9] V. Bužek and M. Hillery, Phys. Rev. A **54**, 1844 (1996).
[10] V. Scarani, S. Iblisdir, N. Gisin, and A. Acín, Rev. Mod. Phys. **77**, 1225 (2005).
[11] A. Lamas-Linares, C. Simon, J. C. Howell, and D. Bouwmeester, Science **296**, 712 (2002).
[12] U. L. Andersen, V. Josse, and G. Leuchs, Phys. Rev. Lett. **94**, 240503 (2005).
[13] S. Liu, Y. Lou, Y. Chen, and J. Jing, Phys. Rev. Lett. **126**, 060503 (2021).
[14] M. A. Nielsen and I. L. Chuang, *Quantum Computation and Quantum Information* (Cambridge University Press, Cambridge, United Kingdom, 2010).
[15] B. M. Terhal, Rev. Mod. Phys. **87**, 307 (2015).
[16] P. W. Shor, Phys. Rev. A **52**, R2493 (1995).
[17] C. H. Bennett, D. P. DiVincenzo, J. A. Smolin, and W. K. Wootters, Phys. Rev. A **54**, 3824 (1996).
[18] A. R. Calderbank and P. W. Shor, Phys. Rev. A **54**, 1098 (1996).
[19] A. M. Steane, Phys. Rev. Lett. **77**, 793 (1996).
[20] S. L. Braunstein, Nature (London) **394**, 47 (1998).
[21] M. Grassl, T. Beth, and T. Pellizzari, Phys. Rev. A **56**, 33 (1997).
[22] C. H. Bennett, D. P. DiVincenzo, and J. A. Smolin, Phys. Rev. Lett. **78**, 3217 (1997).
[23] Y. Wu, S. Kolkowitz, S. Puri, and J. D. Thompson, Nat. Commun. **13**, 4657 (2022).
[24] J. Niset, U. L. Andersen, and N. J. Cerf, Phys. Rev. Lett. **101**, 130503 (2008).
[25] M. Lassen, M. Sabuncu, A. Huck, J. Niset, G. Leuchs, N. J. Cerf, and U. L. Andersen, Nat. Photonics **4**, 700 (2010).
[26] C. Zhong, C. Oh, and L. Jiang, Quantum **7**, 939 (2023).
[27] E. Villaseñor and R. Malaney, *GLOBECOM 2022–2022 IEEE Global Communications Conference, Rio de Janeiro, Brazil* (IEEE, New York, 2022), 5231–5236.
[28] L. Allen, M. W. Beijersbergen, R. J. C. Spreeuw, and J. P. Woerdman, Phys. Rev. A **45**, 8185 (1992).
[29] J. Wang, J. Yang, I. M. Fazal, N. Ahmed, Y. Yan, H. Huang, Y. Ren, Y. Yue, S. Dolinar, M. Tur, and A. E. Willner, Nat. Photonics **6**, 488 (2012).
[30] N. Bozinovic, Y. Yue, Y. Ren, M. Tur, P. Kristensen, H. Huang, A. E. Willner, and S. Ramachandran, Science **340**, 1545 (2013).
[31] S. Liu, Y. Lou, and J. Jing, Nat. Commun. **11**, 3875 (2020).
[32] X. Pan, S. Yu, Y. Zhou, K. Zhang, K. Zhang, S. Lv, S. Li, W. Wang, and J. Jing, Phys. Rev. Lett. **123**, 070506 (2019).
[33] Y. Chen, S. Liu, Y. Lou, and J. Jing, Phys. Rev. Lett. **127**, 093601 (2021).
[34] C. F. McCormick, V. Boyer, E. Arimonda, and P. D. Lett, Opt. Lett. **32**, 178 (2007).
[35] V. Boyer, A. M. Marino, R. C. Pooser, and P. D. Lett, Science **321**, 544 (2008).
[36] A. M. Marino, R. C. Pooser, V. Boyer, and P. D. Lett, Nature (London) **457**, 859 (2009).
[37] R. C. Pooser, A. M. Marino, V. Boyer, K. M. Jones, and P. D. Lett, Phys. Rev. Lett. **103**, 010501 (2009).

[38] S. Liu, Y. Lou, and J. Jing, Phys. Rev. Lett. **123**, 113602 (2019).
[39] A. Einstein, B. Podolsky, and N. Rosen, Phys. Rev. **47**, 777 (1935).
[40] K. Huang, H. Le Jeannic, J. Ruaudel, O. Morin, and J. Laurat, Rev. Sci. Instrum. **85**, 123112 (2014).
[41] See Supplemental Material at http://link.aps.org/supplemental/10.1103/PhysRevLett.132.040601 for the experimental details of experimental setup, the details of theoretical calculation, examining the amplitudes of the input and output, OAM multiplexed entanglement with two pairs of entangled OAM modes, the experimental results with erasure on $\hat{a}_1$ channel when input state codes OAM mode, and the experimental results with erasure on $\hat{a}_2$, $\hat{b}_1$, $\hat{b}_2$ channels, which includes Refs. [42–44].
[42] T.-M. Zhao, Y. S. Ihn, and Y.-H. Kim, Phys. Rev. Lett. **122**, 123607 (2019).
[43] L. M. Duan, G. Giedke, J. I. Cirac, and P. Zoller, Phys. Rev. Lett. **84**, 2722 (2000).
[44] R. Simon, Phys. Rev. Lett. **84**, 2726 (2000).
[45] S. L. Braunstein, C. A. Fuchs, H. J. Kimble, and P. van Loock, Phys. Rev. A **64**, 022321 (2001).
[46] N. Takanashi, A. Inoue, T. Kashiwazaki, T. Kazama, K. Enbutsu, R. Kasahara, T. Umeki, and A. Furusawa, Opt. Express **28**, 34916 (2020).
[47] D. Zhang, C. Li, Z. Zhang, Y. Zhang, Y. Zhang, and M. Xiao, Phys. Rev. A **96**, 043847 (2017).
[48] W. Zhang, N. Jiao, R. Li, L. Tian, Y. Wang, and Y. Zheng, Opt. Express **29**, 24315 (2021).
[49] H. Vahlbruch, M. Mehmet, K. Danzmann, and R. Schnabel, Phys. Rev. Lett. **117**, 110801 (2016).